Research Article | Vol. 9, No. 10 | 1 Oct 2018 | BIOMEDICAL OPTICS EXPRESS 5100
Biomedical Optics EXPRESS

Ciliary muscle thickness profiles derived from optical coherence tomography images

SANDRA WAGNER,[1,*] EBERHART ZRENNER,[1,2] AND TORSTEN STRASSER[1]

[1]*Institute for Ophthalmic Research, Eberhard Karls University Tuebingen, Elfriede-Aulhorn-Str. 7, 72076 Tuebingen, Germany*
[2]*Werner Reichardt Centre for Integrative Neuroscience (CIN), Otfried-Mueller-Str. 25, 72076 Tuebingen, Germany*
**sandra.wagner@uni-tuebingen.de*

Abstract: The purpose of this study was to provide an in-depth analysis of the ciliary muscle's (CM) morphological changes during accommodation by evaluating CM thickness (CMT) profiles. The CM of 15 near-emmetropic subjects (age 20-39) was imaged via optical coherence tomography (OCT) during far (0 D) and near vision (3 D). A custom-made Java-based program was used for semi-automatic CM segmentation and thickness measurements. CMT profiles were generated to determine regions of the largest shape changes. The results revealed on average a thinning within the first 0.25 mm and a thickening from 0.36 to 1.48 mm posterior to scleral spur when accommodating from 0 to 3 D. In contrast to previous analyses, this method offers pixel-wise reconstruction of CM shapes and quantification of accommodative change across the entire muscle boundary.

1. Introduction

Accommodation is the process by which the eye changes the crystalline lens' refractive power to maintain a clear image of objects at different viewing distances. The ciliary muscle, a smooth muscle that consists of three types of muscle fibers [1] is the only active element of this mechanism. It is responsible for changing the shape of the eye lens by reducing the tension of the anterior zonules [2]. Although most important in the accommodation process, the ciliary muscle is still understudied compared to other structures in the human body [3]. However, interest in ciliary muscle biometry has increased during the last decade, especially in presbyopia and myopia research – the former because of new approaches for artificial accommodation using the ciliary muscle's contraction in intraocular lens designs [4,5], the latter because myopia development is thought to be related to near-vision behavior [6–9].

The anatomical structures of the ciliary muscle have previously been studied using ultrasound biomicroscopy [10–14], optical coherence tomography (OCT) [15–28], and magnetic resonance imaging [15,18,29] in emmetropic and myopic subjects. Examinations revealed that the accommodative response correlates with the thickness change of the ciliary muscle, more specifically, that the muscle thickens anteriorly and thins posteriorly with increasing accommodation [16,18,24]. As to differences depending on the refractive error, it was found that an increased thickness of the ciliary muscle is associated with myopia [11,14–16,22] and that in the unaccommodated state, the ciliary muscle is significantly longer in eyes with greater axial length [24]. Moreover, Jeon et al. found that subjects with myopia display a reduced movement of the ciliary muscle during the accommodation process [10]. A relation between myopia development and ciliary muscle anatomy was supported by the suggestion that the ciliary muscle's tonus affects the axial length of the eye by influencing the tension in the choroid [30]. It has been hypothesized that the increased ciliary muscle thickness changes the mechanical properties that impede equatorial stretch, thus promoting myopic development [8].

Previous studies analyzing the ciliary muscle biometry using OCT either took selective readings by measuring the ciliary muscle thickness in equidistant steps of 1 mm posterior to the

#341239 https://doi.org/10.1364/BOE.9.005100
Journal © 2018 Received 31 Jul 2018; revised 18 Sep 2018; accepted 18 Sep 2018; published 1 Oct 2018

Biomedical Optics EXPRESS

scleral spur [15–23,25,31–33], or the muscle thickness was measured proportionally [24,26,27]. Both measurement procedures are subject to limitations: Selective measurements do not consider inter-individual differences in total ciliary muscle length which might lead to different anatomical locations of the muscle at the varying distances posterior to the scleral spur [3]. Proportional measurements require knowledge about the muscle's total length and therefore a clear definition of the muscle's end which is not always feasible due to the resolution limits of the OCT.

Ruggeri and colleagues suggested using small steps of 0.25 mm within the first 1 mm posterior to the scleral spur to enable detailed measurements of thickness changes from far to near vision [21]. We aimed at taking even closer readings by measuring the muscle thickness pixel-wise, corresponding to about 8 µm. The entire muscle boundary is used for thickness measurements, thereby providing a profile of the ciliary muscle thickness, which, taken for different viewing conditions, would allow the definition of individual areas of the largest shape changes during muscle contraction. The above-mentioned limitations of selective and proportional readings thus could be avoided.

The purpose of the current investigation was to provide an in-depth analysis of the ciliary muscle's morphologic changes during accommodation using a newly developed image analysis method. Offering a new approach to investigate the morphologic changes during ciliary muscle contraction, this method could be used in the future for a detailed analysis of the ciliary muscle in emmetropic vs. myopic eyes. Improved methodology would furthermore be beneficial for understanding accommodation as well as the possible role of the ciliary muscle thickness in the development of myopia.

2. Methods

2.1 Subjects

Subjects were recruited from the staff of the Institute for Ophthalmic Research, Eberhard Karls University Tuebingen, Germany. Fifteen near-emmetropic subjects between the ages of 20 and 39 years (29.3 ± 5.1 years) with a mean spherical equivalent refractive error of the right eye of –0.03 ± 0.37 D (range –0.50 to + 0.63 D) were included. Uncorrected distance Snellen visual acuity was at least 6/7.5 (20/25) in each eye. Prior to the measurements, subjects were informed about the aim, the procedure, and possible risks of the study, and thereafter gave their informed consent. Subjects with ocular pathologies or binocular disorders were excluded from the trial. The study followed the tenets of the declaration of Helsinki and was approved by the Institutional Review Board of the medical faculty of the University of Tuebingen.

2.2 Measurement procedure

2.2.1 Pre-measurements

After the anamnesis, including questions regarding general health, an examination of the anterior segment of the subject's eyes was performed by an ophthalmologist to ensure inclusion criterion of ocular health was upheld. Objective refraction was determined using a wavefront aberrometer (Nidek AR-360A, OCULUS Optikgeräte GmbH, Wetzlar, Germany), and subjective refraction was subsequently undertaken using a digital optotype chart monitor (Nidek System Chart SC-1600P, OCULUS Optikgeräte GmbH, Wetzlar, Germany). Subjective refraction adhered to the rule of maximum plus lens for best visual acuity. Monocular visual acuity was tested with and without correction. Moreover, the dominant eye was determined by an eye-sighting method with the hands forming a triangle [34]. The maximum amplitude of accommodation of both eyes was separately measured via the push-up method using the Duane's figure [35].

Biomedical Optics EXPRESS

2.2.2 Ciliary muscle imaging

The temporal ciliary muscle of the right eye was imaged in two different accommodative states using an anterior segment-OCT (Visante, Carl Zeiss Meditec AG, Jena, Germany). The experimental setup is outlined in Fig. 1. Subjects were positioned in front of the instrument with their head placed in a combined head and chin rest. To facilitate imaging of the ciliary muscle in its entirety, it was necessary for subjects to shift their fixation gaze by about 40° while keeping their chin and head at 0°, parallel to the instrument. In this way, the instrument's infrared beam only passes the sclera to reach the ciliary muscle, thereby avoiding the highly pigmented iris [22,26]. The instrument's enhanced high resolution corneal mode with 512 A-scans was chosen, providing a scanning size of 10 mm length and 3 mm tissue depth. Prior to the imaging, subjects were asked to fixate the instrument's internal Maltese cross target to align the instrument with their pupil center. Only after this alignment, subjects shifted their gaze externally. This procedure was chosen because specific landmarks, like the pupil or conjunctival blood vessels normally serving as points of reference during anterior segment or fundus imaging, are missing in ciliary muscle imaging. It was also verified that the subject's gaze did not change vertically when changing from 0° to about 40° eccentrically to fixate the target. This, together with the prior pupil center alignment should ensure maintenance of the same sectional plane during the following measurements.

Subjects fixated an external target with their left eye by looking into a mirror that was attached to the instrument's head rest while OCT imaging was performed on their right eyes. They were successively provided with a near target of 3 D accommodative demand and a far target of 0 D, whereby the sequence was chosen randomly. The near target was presented on a QXGA TFT LCD-display (Adafruit Qualia 9.7" DisplayPort Monitor, Adafruit, New York City, USA) providing a resolution of 2048 x 1536 pixels and a luminance of 440 cd/m^2, which was reduced to about 2 cd/m^2 for stimulus presentation. For the recording of far accommodation, the near display was moved aside, allowing an unobstructed view of the far LCD-monitor (FlexScan EV2736W, EIZO Europe GmbH, Moenchengladbach, Germany; resolution 2560 x 1440 pixels, luminance during target presentation 50 cd/m^2) which was placed in the same alignment axis as the near display. Prior to the beginning of the study, far and near display were aligned for one subject, to avoid a shift in gaze when switching between targets. Having marked the exact position of the near display, it was repositioned at the same place for the imaging of the following subject and adjusted individually if necessary. The subject's accommodative response was simultaneously measured by a custom-built eccentric infrared photorefractor [36,37]. Accommodative responses were measured during the whole imaging procedure at both target distances, respectively. The photorefractor was positioned at a distance of 1 m at an angle of about 40° to the subject. Recordings of the subject's left eye's accommodation response were taken through the small gap between mirror and head rest (Fig. 1). Empirical calibration values were applied as only relative refractive power changes during accommodation were to be analyzed. Refraction was measured in the vertical meridian with a sampling frequency of 100 Hz. Time stamps of OCT images and photorefractor software were used to correlate the recordings. Room illuminance during the imaging procedure was about 20 lux to achieve pupil sizes of more than 4 mm.

Biomedical Optics EXPRESS

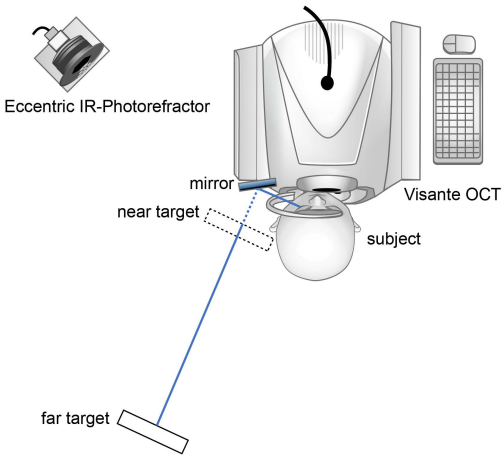

Fig. 1. Experimental setup. Subjects were positioned in front of the OCT with their head in 0° and their fixation gaze shifted by about 40°. With their left eye, subjects fixated a target through a mirror which was attached to the head rest while their right eye's ciliary muscle was imaged. For far vision, the near display was moved out of the subjects' fixation line to allow unobstructed view of the far target. The order of target presentation was randomized. Simultaneous measurements of accommodative response were undertaken by eccentric infrared photorefraction.

A continuous text in white font on a black background, with the central letter colored in red, was chosen as a fixation target for both near and far accommodation. To allow the subject to follow the content of the text, it was presented continuously, so that the targets during far and near vision were not the same. Single words with a constant position on the display were presented successively with a frequency of 2 Hz. Fixating the central colored letter still allowed reading the entire word. This rapid serial visual presentation (RSVP) was chosen to reduce eye movements during measurements and to keep the accommodation accuracy high. The custom-made RSVP program was written in PsychoPy [38]. Sloan font [39] with a letter size equivalent to a visual acuity of Snellen 6/15 (20/50), corresponding to a visual angle of 2.5 min of arc for the critical detail, was used at each target distance to induce accurate accommodation.

To increase the signal-to-noise ratio, six OCT images were taken during far and near accommodation, respectively. For both target distances, the subjects were given a short break after the recording of three images, and they were realigned in front of the device for the following three images. This procedure allowed the evaluation of intra-session repeatability.

2.3 Software for semi-automatic segmentation and dimensional measures

Raw DICOM images of the Visante software, with a refractive index of 1.0, were exported, rotated, and resized to 1280 x 512 pixels [31] for further analysis. Semi-automatic segmentation of the ciliary muscle was performed using a custom-made Java-based (Oracle Corporation, Redwood Shores, CA, USA) software: In the first step, landmarks were placed manually along the border of the ciliary muscle (Fig. 2(A)). Examiners were asked to distribute the landmarks evenly along the muscle border. These landmarks were used for fitting polynomial splines as rough muscle boundaries. Subsequently, within a band of five pixels on each side of the boundaries, the maximum brightness gradient was determined and taken for a second, accurate fit of the boundaries, again using polynomial splines (Fig. 2(B)). To achieve a good polynomial fit, landmarks had to be placed more densely in areas of poor image contrast in the regions of the scleral spur and ciliary apex. Both the boundaries of the anterior chamber and the corneal-air boundary were segmented by applying a simple flood fill algorithm using a fraction of the mean luminance as threshold. The borders of the identified area were used as input for the

Biomedical Optics EXPRESS

polynomial spline fit. Finally, refraction distortion correction was undertaken by ray-tracing and implementation of Snell's law [21] applying a custom-made algorithm (Fig. 2(C)). For this calculation, refractive indices of 1.41 and 1.38 were used for sclera and ciliary muscle, respectively [16–18,25,26,31–33]. To provide an anatomical scale, a pixel to millimeter conversion was done with a conversion factor of 128 px/mm as denoted by the manufacturer. Verification of this factor, performed by imaging and analyzing a steel tube of a known diameter (6 mm), resulted in a factor of 130.5 px/mm, which was less than 2% different from the manufacturer's information. For the following calculations, the conversion factor of 128 px/mm was therefore used.

After the refraction distortion correction, the polynomial splines' intersections were used to determine essential points of interest (Fig. 2(B)): The intersection of the upper (1) and the vertical polynomial spline (2) resulted in the scleral spur (SP), intersections of vertical (2) and lower polynomial spline (3) in the ciliary muscle apex (CA), and the iridocorneal angle was derived from the intersection of the two splines marking cornea and iris (yellow in Fig. 2(B)). A selective reading of the ciliary muscle thickness (CMT) was defined as the line segment being perpendicular to the upper ciliary muscle border and crossing the ciliary muscle apex (referred to as "perpendicular axis", Fig. 3). The ciliary muscle area (CMA) was calculated up to 4 mm posterior to the scleral spur, being measured as arc length along the muscle's curvature (Fig. 2(D)). Most importantly, the muscle shape was reconstructed pixel-wise allowing the plotting of CMT profiles. For CMT profiling, a coordinate system originating in the position of the scleral spur was defined. Plotting was accordingly undertaken by subtracting the scleral spur's x coordinate from each x coordinate to shift the entire diagram and set the origin to the scleral spur's position. The x coordinate was derived from the intersection of the perpendiculars to the scleral curvature with the upper ciliary muscle border. The CMT, plotted on the ordinate, was calculated as the distance between the upper and lower ciliary muscle border, whose prolongation was perpendicular to the scleral border (Fig. 3).

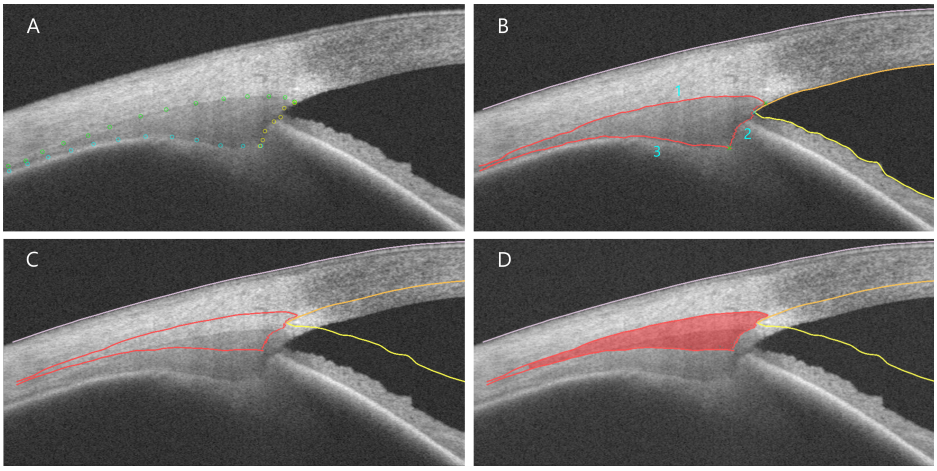

Fig. 2. Semi-automatic segmentation. (A) Manual landmark positioning, (B) Definition of CM boundaries using polynomial splines (1: upper, 2: vertical, 3: lower CM border); points of interest are labeled with a green cross, (C) New CM boundaries after refraction distortion correction, (D) Calculation of CM area (red).

Biomedical Optics EXPRESS

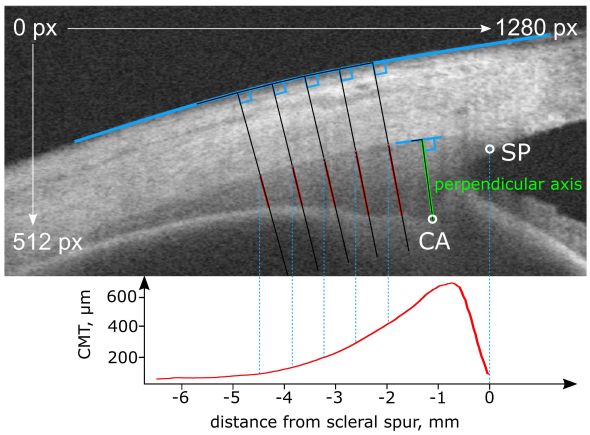

Fig. 3. Definition of morphological measures. OCT image of CM with sketch illustrating the plotting of CM thickness profiles and the definition of the perpendicular axis (green line).

2.4 Data processing and image analysis

OCT images were analyzed in a masked, randomized way to avoid any bias regarding expected thickness changes due to accommodation.

Refractive power measurements taken by the eccentric photorefractor were filtered for blink artefacts using a function written in Matlab Version R2017a (The Mathworks GmbH, Ismaning, Germany) and averaged for each subject during both viewing tasks, respectively.

2.4.1 Regions of largest change

The thresholds determining a 'large change' in CMT were derived from the instrument's axial resolution, which is 18 µm, corresponding to about 2.304 px. Regions of largest thickness changes for all subjects were defined by calculating the average difference in CMT between far and near accommodation (Δ thickness(far-near)) and by applying a bivariate fit with Kernel smoothing (alpha = 0.056) to the graph. The intersections of the fit with the ± 18 µm thresholds were then used to determine the boundaries of the regions of largest shape changes.

2.4.2 Distance of scleral spur to ciliary muscle apex

To analyze the ciliary muscle's movement during accommodation, the Euclidean distance between the scleral spur and the ciliary muscle apex during far vs. near accommodation was calculated from the pixel coordinates of the points in each image. The average distance per subject and accommodation demand was thereafter calculated and converted to mm.

2.4.3 Shift of the ciliary muscle apex during accommodation

The horizontal shift of the ciliary muscle apex' position against the scleral spur from far to near accommodation was calculated by (1) defining the tangent line to the sclera at the scleral spur, (2) placing the perpendicular line to this tangent line (q), (3) drawing the perpendicular line to q passing through the ciliary muscle apex (d_F and d_N). The x-values d_F and d_N ultimately define the ciliary muscle apex' change in position (Fig. 4).

Biomedical Optics EXPRESS

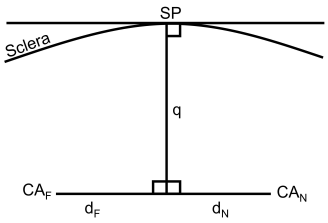

Fig. 4. Horizontal shift of the ciliary muscle apex' position against the scleral spur. Graphical derivation to calculate the horizontal displacement of the ciliary muscle apex' position (CA) against the scleral spur's position (SP) for far (d_F) and near accommodation (d_N).

2.5 Repeatability analysis

To evaluate intra-examiner repeatability, one examiner performed the landmark positioning for the semi-automatic segmentation twice in a masked way at an interval of one week. The average of the CMA over the six measurements in both target distances was calculated and analyzed for both evaluations, respectively. Intra-session repeatability was analyzed for both target distances by averaging and comparing the CMA of the first three and the last three images taken per subject, respectively. Inter-examiner repeatability was additionally performed by comparing the averaged CMA at both distances derived from separate landmark positioning of two examiners.

2.6 Statistical analysis

Statistical analysis was undertaken using JMP 14 (SAS Institute GmbH, Heidelberg, Germany) and IBM SPSS Statistics 24 (IBM Deutschland GmbH, Ehningen, Germany). Repeatability analysis was performed by means of a paired t-test and Bland-Altman plots, and the intraclass correlation was additionally investigated.

3. Results

The subjects' mean amplitude of accommodation was found to be 7.33 ± 1.23 D for the right eye and 7.49 ± 1.33 D for the left. Due to poor OCT image quality and therefore a lack of evaluable image material in two subjects, they were excluded from the analysis, leaving the study cohort with a total of 13 subjects. Refractive power measurements by eccentric photorefraction were not possible in two subjects because of difficulties with pupil tracking: the eyelid either partly covered the pupil or the pupil diameter was considerably reduced during near accommodation, both preventing reliable measurements of refractive power by photorefraction.

3.1 Repeatability analysis

3.1.1 Intra-examiner repeatability

The averaged CMA, calculated for each subject at both distances, was significantly different between the two successively performed ciliary muscle segmentations. Results of the paired t-test demonstrated a statistically significant difference between the averaged CMA of both segmentations ($t_{25} = -2.806$, $p = 0.010$, two-tailed; mean difference −0.06 ± 0.10 mm^2; $mean_{Seg\_1}$: 1.26 ± 0.16 mm^2; $mean_{Seg\_2}$: 1.21 ± 0.16 mm^2). The Bland-Altman analysis (Fig. 5 left) visualizes the differences between the repeated evaluations and shows that the CMA was larger in the first segmentation.

To allow a comparison of these deviations to the instrument's resolution which cannot be readily realized using the CMA, it was additionally tested how much the perpendicular axis varied between the repeated landmark positionings. Although a paired t-test also resulted in a significant difference between the mean perpendicular axis of both segmentations ($t_{25} = 6.049$,

Biomedical Optics EXPRESS

p<0.0001, two-tailed), the data showed that the mean difference between the repeated measures was 22.97 ± 19.36 µm, corresponding to only 2.94 px.

Taking into consideration a presumable learning effect in landmark positioning, the following analysis is based on the second segmentation of the first examiner which showed a more consistent approach in segmenting.

3.1.2 Intra-session repeatability

Intra-session repeatability derived from analyzing the averaged CMA of the first three vs. the last three OCT images for each subject was found to be good with an ICC of 0.879 (95% confidence intervals 0.724 to 0.947). A paired t-test revealed no significant difference (t_{24} = 0.054, p = 0.957, two-tailed, mean difference 0.001 ± 0.120 mm^2). This was confirmed via the Bland-Altman analysis (Fig. 5 middle). The mean difference between the perpendicular axis of the first three vs. the last three images was 6.17 ± 23.67 µm. The perpendicular axis and the CMA separately calculated for far and near accommodation are provided in Table 1, whereby the values of the first three and the last three images taken within one measurement session were averaged over the 13 subjects, respectively.

Table 1. Intra-session repeatability. Comparison of anatomical values averaged over all subjects for the first three vs. the last three images taken within one session for far and near accommodation, respectively.

		mean of images 1-3	mean of images 4-6	difference
CMA, mm²	far	1.1632	1.1607	0.0025
	near	1.2413	1.2504	-0.0091
perpendicular axis, µm	far	656.74	653.58	3.16
	near	702.34	693.83	8.51

3.1.3 Inter-examiner repeatability

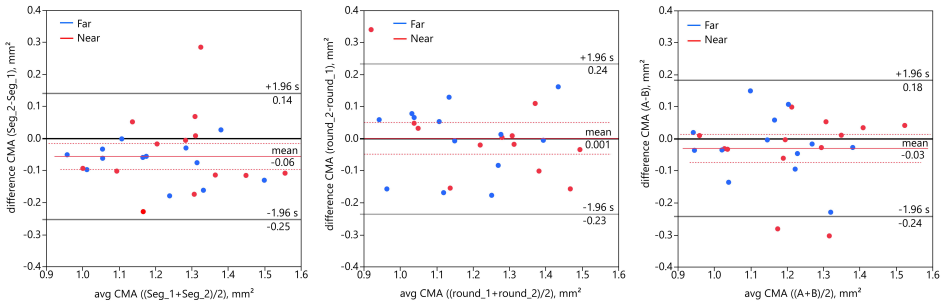

Fig. 5. Left: Intra-examiner repeatability of first (Seg_1) and second (Seg_2) segmentation. Bland-Altman plot showing the difference between the repeated CMA evaluation for both distances (blue circles: 0 D, red circles: 3 D) as a function of the mean, with mean difference (solid red line) and 95% confidence intervals (dotted red line). Grey solid lines denote limits of agreement (mean difference ± 1.96 * SD of difference). Middle: Intra-session repeatability of first (round_1) and second (round_2) imaging. Bland-Altman plot showing the difference between averaged CMA of first three and last three images of one individual session. Right: Inter-examiner repeatability of examiner A and examiner B. Bland-Altman analysis reveals good inter-examiner repeatability with a mean difference of –0.03 mm^2.

Inter-examiner repeatability was assessed by calculating the averaged CMA in OCT images which were segmented by two independent examiners. The second examiner was not naive to landmark positioning. Comparing the CMA resulting from the second landmark positioning of the first examiner and from the segmentation by the second examiner revealed good inter-

Biomedical Optics EXPRESS

examiner repeatability (paired t-test $t_{25} = -1.384$, $p = 0.179$), with an ICC of 0.868 (95% confidence intervals 0.710 to 0.941). The mean difference between both segmentations was -0.03 ± 0.11 mm^2 (Fig. 5 right; mean$_A$: 1.18 ± 0.16 mm^2; mean$_B$: 1.21 ± 0.16 mm^2).

3.2 Ciliary muscle thickness profiles

Applying a bivariate fit with Kernel smoothing (alpha = 0.056) to the CMT differences between far and near accommodation and taking the OCT's axial resolution of 18 µm as threshold as described in section 2.4.1, the averaged CMT profiles revealed two main regions of largest change (Fig. 6): When changing from far to near accommodation, the ciliary muscle showed a thinning predominantly within 0.00 to 0.25 mm from the scleral spur and a thickening in the region from 0.36 to 1.48 mm.

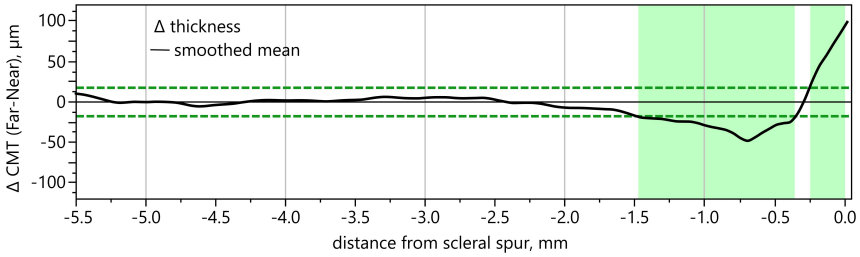

Fig. 6. Definition of region of largest thickness change. Using a bivariate fit with Kernel smoothing (black line) for the CMT difference between far and near accommodation and taking 18 µm as thresholds (derived from axial resolution of OCT; green dashed lines), two regions of largest thickness changes were identified, the first between 0.00 to 0.25 mm, and the second between 0.36 to 1.48 mm (green bars).

The CMT profiles for far and near accommodation, averaged over all subjects, are shown in Fig. 7, with coloring of the two regions with the largest thickness changes. The profiles were plotted using the position of the scleral spur as the origin.

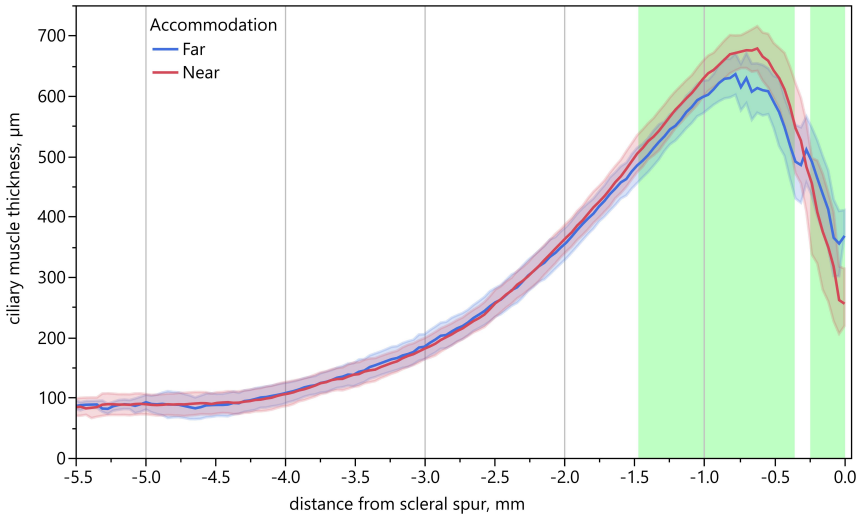

Fig. 7. Averaged CMT profiles for far and near accommodation. Averaged CMT for far (blue) and near accommodation (red), respectively, using the coordinate system with origin in the scleral spur position. Shaded areas denote ± 1 SD. Green bars indicate regions of largest thickness change.

Biomedical Optics EXPRESS

The analysis of the in section 2.3 defined selective measures of the perpendicular axis revealed a significant difference between the average values for far and near accommodation (paired t-test $t_{12} = 3.484$, $p = 0.0045$, two-tailed), with significantly thicker muscles during near accommodation ($\Delta_{far\text{-}near} = -43.04$ µm).

3.3 Movement of ciliary muscle during accommodation

Evaluation of the displacement of the ciliary muscle apex vs. the scleral spur confirmed the muscle's forward and inward movement during accommodation: The ciliary muscle apex was positioned 0.52 ± 0.26 mm in front of the scleral spur during far vision and shifted to 0.16 ± 0.36 mm behind the scleral spur during near vision (paired t-test, $t_{12} = -6.172$, $p<0.001$, two-tailed). While the distance between the ciliary muscle apex and the scleral spur was 0.92 ± 0.15 mm for far vision, it decreased to 0.85 ± 0.10 mm for 3 D accommodation.

3.4 Individual CMT profiles

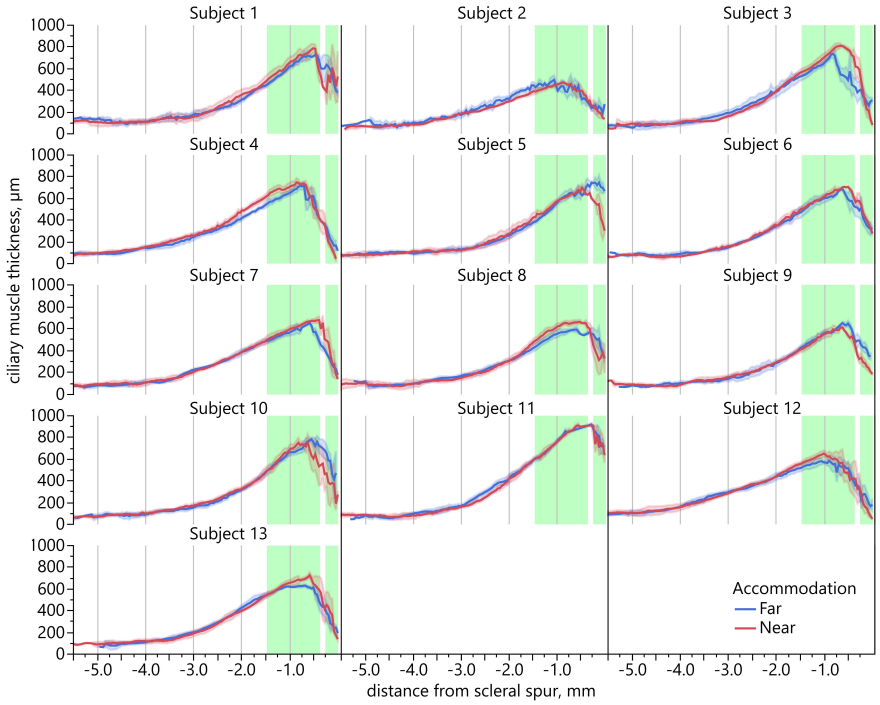

Fig. 8. Individual CMT profiles. CMT profiles of all 13 subjects with CMT during far (blue line) and during near vision (red line). Green bars represent average regions of largest CMT change. Shaded areas denote ± 1 SD of repeated imaging per subject.

The individual plotting of CMT profiles revealed large inter-individual differences in the CMT changes from far to near accommodation with some of them deviating considerably from the average plot (Fig. 8). Subjects 1, 3, 4, 8, 10, 12, and 13 show similar CMT changes as the average, however with different areas of largest change, as can be seen when referring to the green average bars in the individual plots. In contrast, the CMT profiles of subjects 5, 6, 7, and 9 demonstrate only one area of thickness change: Subjects 5 and 9 display a thicker ciliary muscle for far than for near vision in the region 0.75 mm posterior to the scleral spur, while subjects 6 and 7 show a thicker ciliary muscle for near than for far vision in the same region posterior to the scleral spur. Interestingly, subject 2 shows a thicker CMT for far vision from 1.0 mm to 3.0 mm posterior to the scleral spur. Within 0.75 to 1.0 mm, the ciliary muscle is thicker for near vision, and within the first 0.25 mm from scleral spur, CMT is again larger for

Biomedical Optics EXPRESS

far vision. Subject 11 does not seem to change his CMT when accommodating 3 D. Only in the region 2.0 to 4.5 mm posterior to the scleral spur, the ciliary muscle is thicker for far vision. However, a more detailed look at this subject's accommodation response taken by eccentric photorefraction confirms that the subject provided an appropriate increase of refractive power for near vision. The same applies to subject 2, who, despite the opposite CMT changes, increases his accommodation by about 3 D during near vision. The average accommodation change from far to near vision of the 11 subjects of whom photorefractor readings were taken was −3.04 ± 1.64 D.

3.5 Individual selective CMT readings

The perpendicular axis during far and near accommodation of the 13 individuals is shown in Table 2. The values confirm the inter-individual variability, with some subjects showing no difference in their perpendicular axis when accommodating from 0 D to 3 D, such as subject 2, while others exhibit an increase of CMT by more than 100 µm during near vision (subject 3). In contrast to all other participants, subject 5 shows a decrease of CMT when changing accommodation from far to near vision. Due to the subject's strong pupil near response, accommodative measurements by eccentric photorefraction to verify the refractive power changes were not possible. However, the subject indicated that he had seen the words on the near display clearly. Table 2 additionally shows that not only the amount of the perpendicular axis varies from subject to subject, but also its variability during repeated measures, with standard deviations ranging from 13.1 µm in subject 9 to 74.7 µm in subject 3.

Table 2. Individual perpendicular axis for far and near accommodation for all 13 subjects

Subject	perpendicular axis, µm				
	Far		Near		Δ Far-Near
	mean	SD	mean	SD	
1	713.3	47.8	767.7	37.6	–54.4
2	476.4	40.4	476.2	13.8	0.2
3	684.5	74.7	786.9	39.3	–102.4
4	730.5	26.0	756.4	23.3	–25.9
5	700.3	52.7	643.2	41.4	57.1
6	645.8	28.7	691.4	25.6	–45.6
7	595.9	43.3	667.2	43.3	–71.3
8	575.0	26.4	653.9	15.3	–78.9
9	587.9	13.1	596.7	24.6	–8.8
10	740.0	48.6	789.3	41.6	–49.3
11	856.1	22.9	866.4	45.0	–10.3
12	597.5	30.8	676.0	42.0	–78.5
13	620.1	23.1	711.3	28.4	–91.2

4. Discussion

Enhanced knowledge about the ciliary muscle's morphological structures would be instrumental in better understanding the accommodation behavior, and therefore foster both presbyopia and myopia research. Compared to other ciliary muscle imaging techniques, OCT is a non-invasive, timesaving, and affordable approach to study the ciliary muscle and can therefore be readily used in large study cohorts and is suited for children.

The purpose of the current study was to test a new analysis method for OCT images of the ciliary muscle, providing thickness profiles instead of selective or proportional measurements. The ciliary muscle of 13 near-emmetropic subjects was analyzed regarding its thickness changes and its movement during accommodation.

Biomedical Optics EXPRESS

4.1 Ciliary muscle analysis by CMT profiling

Plotting the CMT along its length allows a detailed analysis and comparison of subjects' ciliary muscles without the need for making a priori assumptions on their anatomical scales. In contrast to previous studies, it is neither necessary to know the muscle's entire length, a limiting factor of proportional measures, nor does this analysis rely on comparing the ciliary muscle of different subjects at the same distance to the scleral spur, which could result in different anatomical positions. By defining the scleral spur as the origin of the coordinate system, it is possible to lay multiple CMT profiles of several subjects on top of each other, with the scleral spur as anchor. The chosen coordinate system makes the CMT readings independent of the individual image section and of the muscle's position and orientation within the image. Thereby, changes between several subjects, but also inner-subject differences for various accommodative demands can be visualized and analyzed.

While previous studies analyzing the ciliary muscle using OCT found a thinning of the muscle at a measurement position 3.0 mm posterior to the scleral spur [16,17,24,32], this could not be confirmed by the current averaged CMT profiles. When taking the bivariate fit of the muscle profile and the axial instrument resolution as cutoff, thickness changes were only present within the first 2.0 mm posterior to the scleral spur, on average, including both a thinning and a thickening region. However, the analysis of the 13 CMT profiles demonstrates that on an individual basis, it is also possible to identify CMT differences in the region 3.0 mm posterior to the scleral spur and beyond. In addition, deviations from previous investigations could arise from methodological differences: Lossing and colleagues, as well as Richdale et al., analyzed the CMT change from 0 D to 4 D [17,32], Sheppard and Davies investigated the CMT change from 0.19 D to 4 D accommodative demand, as well as from 4 D to 8 D [24], and Lewis et al. applied accommodative demands of 4 D and 6 D [16]. Not only the accommodation demand, but also the instrument and its resolution, the sample size, and the subject's age varied across these studies. Analyzing the CMT changes of one 45-year-old subject when accommodating from 0 to 6 D, Ruggeri et al. found the largest changes in the area 0.75 mm posterior to the scleral spur [21]. The measured differences are in the same range as the ones of the current trial, even though the accommodative demand was doubled. Whether this evolves from the difference in subject age or in methodology and applied instrument is not clear. In their following study, Ruggeri and colleagues measured a larger CMT change in a 45-year-old subject than in a 22-year-old for 2 D of accommodation demand [19]. Richdale et al. however did not find a significant difference in CMT with age [18].

Comparison of the here presented individual CMT profiles and the numeric data of the perpendicular axis disclose that both measures do not necessarily result in the same conclusion. This can particularly be seen in subject 2, whose perpendicular axis did not change from far to near vision, while the CMT profile reveals differences in the CMT for 0 D and 3 D. Taking this into consideration, it might not be sufficient to judge a subject's ciliary muscle behavior only by selective measures as has been done in previous trials.

4.2 Possible limitations

Analysis of the repeated landmark positioning demonstrated that the semi-automatic segmentation procedure might lead to deviations between repeated measures in the order of the instrument's resolution. In view of a possible learning effect of the examiner throughout the process of landmark positioning, the ciliary muscle analysis should be undertaken by an experienced examiner. In case of small sample sizes, the analysis should be done by the same examiner instead of being apportioned among several investigators.

Variability in the CMT readings could have partly arisen from limitations of the experimental setup used in this study. The need for moving the display during the measurement session could have led to a slight change in the subject's gaze and thereby to a change in the scanning sectional plane. Moreover, small movements of the subjects during imaging might have resulted in a non-alignment to the thickest horizontal slice of the ciliary muscle. This in

Biomedical Optics EXPRESS

turn might have contributed to ciliary muscle changes that were either very low or opposite of expected as found in subject 11 and subject 2, respectively. The low accommodation demand of only 3 D could have prevented the detection of larger CMT changes. It is well-known that the mean pupil diameter decreases with age [40], and regarding the strong pupil near response in some subjects, it is probable that they were too old to allow consistent readings during near vision using the eccentric photorefractor, as pupil diameters above 4 mm are required.

One could argue that it is not accurate to take the intersections of the polynomial splines to define the points of interest such as scleral spur and ciliary muscle apex. However, a detailed investigation of the segmented and analyzed OCT images revealed that the intersections were consistent with those points that would have been selected manually for scleral spur and apex. This probably results from the fact that landmarks were placed closer to each other in that region.

A fully automatic segmentation software would be eligible to avoid the influence of a possible examiner's learning effect and to thereby render the analysis entirely objective. A conceivable approach would be the use of deep learning networks to conduct the segmentation without the necessity of examiner's input.

It should be emphasized that the conclusions drawn here only apply to the presented results of the 13 subjects measured and do not yet allow a general statement. A much larger sample size is needed to confirm the findings regarding the areas of largest ciliary muscle shape changes and the muscle's movement during accommodation. The application of the presented analysis tool in a larger study population would lead to more general conclusions about the ciliary muscle behavior during accommodation.

5. Conclusion

We present a novel, semi-automatic approach for analyzing the ciliary muscle's anatomy using OCT that facilitates the formation of CMT profiles and the definition of areas of largest change during accommodation, rather than taking selective or proportional readings. Repeatability analysis disclosed consistency within one cycle, but a possible examiner's training effect in segmenting over time, requiring some practice prior to using the semi-automatic technique. With experience in placing landmarks, the segmentation seems to be independent of the investigator as shown by the good inter-examiner repeatability. We aim to apply this tool for an in-depth comparison of ciliary muscle morphology in young adult subjects with myopia vs. emmetropia. Considering the suggestion of a link between near-vision behavior and myopia development, we strive to contribute to a better understanding of the accommodation process in emmetropes vs. myopes.

6. Supplementary material

The software used in the study can be provided upon request.

Funding

Sandra Wagner acknowledges support from the Hector Fellow Academy. Eberhart Zrenner was supported by the German Research Council in the Excellence Center Program (EXC307).

Acknowledgments

We thank Frank Schaeffel for helpful discussions of this project, Fadi Nasser for performing the ophthalmic examinations, and Marco Ruggeri for advice regarding the analysis software. We acknowledge support by the German Research Foundation and the Open Access Publishing Fund of the University of Tuebingen.

Disclosures

The authors declare that there are no conflicts of interest related to this article.

Biomedical Optics EXPRESS

References

1. E. R. Tamm and E. Lütjen-Drecoll, "Ciliary Body," Microsc. Res. Tech. **33**(5), 390–439 (1996).
2. K. J. Ciuffreda, "Accommodation, the pupil, and presbyopia," in *Borish's Clinical Refraction*, W. J. Benjamin, ed. (Butterworth-Heinemann Elsevier Inc., 2006), pp. 93–144.
3. M. D. Bailey, "How should we measure the ciliary muscle?" Invest. Ophthalmol. Vis. Sci. **52**(3), 1817–1818 (2011).
4. J. S. Pepose, J. Burke, and M. Qazi, "Accommodating intraocular lenses," Asia Pac. J. Ophthalmol. **6**(4), 350–357 (2017).
5. O. Findl and C. Leydolt, "Meta-analysis of accommodating intraocular lenses," J. Cataract Refract. Surg. **33**(3), 522–527 (2007).
6. I. Morgan and K. Rose, "How genetic is school myopia?" Prog. Retin. Eye Res. **24**(1), 1–38 (2005).
7. I. G. Morgan and K. A. Rose, "Myopia and international educational performance," Ophthalmic Physiol. Opt. **33**(3), 329–338 (2013).
8. D. O. Mutti, "Hereditary and Environmental Contributions to Emmetropization and Myopia," Optom. Vis. Sci. **87**(4), 255–259 (2010).
9. J. C. Chen, K. L. Schmid, and B. Brown, "The autonomic control of accommodation and implications for human myopia development: a review," Ophthalmic Physiol. Opt. **23**(5), 401–422 (2003).
10. S. Jeon, W. K. Lee, K. Lee, and N. J. Moon, "Diminished ciliary muscle movement on accommodation in myopia," Exp. Eye Res. **105**, 9–14 (2012).
11. C. Oliveira, C. Tello, J. M. Liebmann, and R. Ritch, "Ciliary body thickness increases with increasing axial myopia," Am. J. Ophthalmol. **140**(2), 324–325 (2005).
12. O. Stachs, H. Martin, A. Kirchhoff, J. Stave, T. Terwee, and R. Guthoff, "Monitoring accommodative ciliary muscle function using three-dimensional ultrasound," Graefes Arch. Clin. Exp. Ophthalmol. **240**(11), 906–912 (2002).
13. A. Bacskulin, U. Bergmann, Z. Horóczi, and R. Guthoff, "Kontinuierliche ultraschallbiomikroskopische Darstellung der akkommodativen Veränderung des humanen Ziliarkörpers," Klin. Monatsbl. Augenheilkd. **207**(10), 247–252 (1995).
14. O. Muftuoglu, B. M. Hosal, and G. Zilelioglu, "Ciliary body thickness in unilateral high axial myopia," Eye (Lond.) **23**(5), 1176–1181 (2009).
15. H. Buckhurst, B. Gilmartin, R. P. Cubbidge, M. Nagra, and N. S. Logan, "Ocular biometric correlates of ciliary muscle thickness in human myopia," Ophthalmic Physiol. Opt. **33**(3), 294–304 (2013).
16. H. A. Lewis, C. Y. Kao, L. T. Sinnott, and M. D. Bailey, "Changes in ciliary muscle thickness during accommodation in children," Optom. Vis. Sci. **89**(5), 727–737 (2012).
17. L. A. Lossing, L. T. Sinnott, C. Y. Kao, K. Richdale, and M. D. Bailey, "Measuring changes in ciliary muscle thickness with accommodation in young adults," Optom. Vis. Sci. **89**(5), 719–726 (2012).
18. K. Richdale, L. T. Sinnott, M. A. Bullimore, P. A. Wassenaar, P. Schmalbrock, C. Y. Kao, S. Patz, D. O. Mutti, A. Glasser, and K. Zadnik, "Quantification of age-related and per diopter accommodative changes of the lens and ciliary muscle in the emmetropic human eye," Invest. Ophthalmol. Vis. Sci. **54**(2), 1095–1105 (2013).
19. M. Ruggeri, C. de Freitas, S. Williams, V. M. Hernandez, F. Cabot, N. Yesilirmak, K. Alawa, Y. C. Chang, S. H. Yoo, G. Gregori, J. M. Parel, and F. Manns, "Quantification of the ciliary muscle and crystalline lens interaction during accommodation with synchronous OCT imaging," Biomed. Opt. Express **7**(4), 1351–1364 (2016).
20. K. E. Schultz, L. T. Sinnott, D. O. Mutti, and M. D. Bailey, "Accommodative fluctuations, lens tension, and ciliary body thickness in children," Optom. Vis. Sci. **86**(6), 677–684 (2009).
21. M. Ruggeri, V. Hernandez, C. de Freitas, F. Manns, and J. M. Parel, "Biometry of the ciliary muscle during dynamic accommodation assessed with OCT," Ophthalmic Technol. XXIV Int. Soc. Opt. Photonics **8930**, 89300W (2014).
22. M. D. Bailey, L. T. Sinnott, and D. O. Mutti, "Ciliary body thickness and refractive error in children," Invest. Ophthalmol. Vis. Sci. **49**(10), 4353–4360 (2008).
23. Y. Shao, A. Tao, H. Jiang, M. Shen, J. Zhong, F. Lu, and J. Wang, "Simultaneous real-time imaging of the ocular anterior segment including the ciliary muscle during accommodation," Biomed. Opt. Express **4**(3), 466–480 (2013).
24. A. L. Sheppard and L. N. Davies, "In vivo analysis of ciliary muscle morphologic changes with accommodation and axial ametropia," Invest. Ophthalmol. Vis. Sci. **51**(12), 6882–6889 (2010).
25. A. D. Pucker, L. T. Sinnott, C. Y. Kao, and M. D. Bailey, "Region-specific relationships between refractive error and ciliary muscle thickness in children," Invest. Ophthalmol. Vis. Sci. **54**(7), 4710–4716 (2013).
26. D. S. Laughton, B. J. Coldrick, A. L. Sheppard, and L. N. Davies, "A program to analyse optical coherence tomography images of the ciliary muscle," Cont. Lens Anterior Eye **38**(6), 402–408 (2015).
27. A. L. Sheppard and L. N. Davies, "The effect of ageing on in vivo human ciliary muscle morphology and contractility," Invest. Ophthalmol. Vis. Sci. **52**(3), 1809–1816 (2011).
28. Y. C. Chang, K. Liu, F. Cabot, S. H. Yoo, M. Ruggeri, A. Ho, J. M. Parel, and F. Manns, "Variability of manual ciliary muscle segmentation in optical coherence tomography images," Biomed. Opt. Express **9**(2), 791–800 (2018).
29. S. A. Strenk, J. L. Semmlow, L. M. Strenk, P. Munoz, J. Gronlund-Jacob, and J. K. DeMarco, "Age-related changes in human ciliary muscle and lens: a magnetic resonance imaging study," Invest. Ophthalmol. Vis. Sci.

Biomedical Optics EXPRESS

40(6), 1162–1169 (1999).
30. G. W. H. M. van Alphen, "Choroidal stress and emmetropization," Vision Res. **26**(5), 723–734 (1986).
31. C. Y. Kao, K. Richdale, L. T. Sinnott, L. E. Grillott, and M. D. Bailey, "Semiautomatic extraction algorithm for images of the ciliary muscle," Optom. Vis. Sci. **88**(2), 275–289 (2011).
32. K. Richdale, M. D. Bailey, L. T. Sinnott, C. Y. Kao, K. Zadnik, and M. A. Bullimore, "The effect of phenylephrine on the ciliary muscle and accommodation," Optom. Vis. Sci. **89**(10), 1507–1511 (2012).
33. M. K. Kuchem, L. T. Sinnott, C.-Y. Kao, and M. D. Bailey, "Ciliary muscle thickness in anisometropia," Optom. Vis. Sci. **90**(11), 1312–1320 (2013).
34. D. Lopes-Ferreira, H. Neves, A. Queiros, M. Faria-Ribeiro, S. C. Peixoto-de-Matos, and J. M. González-Méijome, "Ocular dominance and visual function testing," BioMed Res. Int. **2013**, 238943 (2013).
35. T. Kohnen, M. Baumeister, and A. Strenger, "Akkommodationsprüfung," in *Augenärztliche Untersuchungsmethoden*, P. Kroll, M. Kuechle, and H. J. Kuechle, eds. (Georg Thieme Verlag, 2008), pp. 102–106.
36. F. Gekeler, F. Schaeffel, H. C. Howland, and J. Wattam-Bell, "Measurement of astigmatism by automated infrared photoretinoscopy," Optom. Vis. Sci. **74**(7), 472–482 (1997).
37. F. Schaeffel, H. Wilhelm, and E. Zrenner, "Inter-individual variability in the dynamics of natural accommodation in humans: relation to age and refractive errors," J. Physiol. **461**(1), 301–320 (1993).
38. J. W. Peirce, "PsychoPy-Psychophysics software in Python," J. Neurosci. Methods **162**(1-2), 8–13 (2007).
39. D. G. Pelli, J. G. Robson, and A. J. Wilkins, "The design of a new letter chart for measuring contrast sensitivity," Clin. Vis. Sci. **2**(3), 187–199 (1988).
40. I. E. Loewenfeld, "Development and Aging," in *The Pupil. Anatomy, Physiology, and Clinical Applications* (Wayne State University Press, 1993), pp. 498–517.